THE ASTROPHYSICAL JOURNAL, 383:401–406, 1991 December 10

FIRST ABSOLUTE WIND MEASUREMENTS IN THE MIDDLE ATMOSPHERE OF MARS

EMMANUEL LELLOUCH,[1] JEFFREY J. GOLDSTEIN,[2] STEPHEN W. BOUGHER,[3]
GABRIEL PAUBERT,[4] AND JAN ROSENQVIST[1]

Received 1991 March 11; accepted 1991 June 11

ABSTRACT

The first absolute wind measurements in the middle atmosphere of Mars (40–70 km) were obtained from Doppler shifts in the $J = 2$–1 CO transition at 230.538 GHz. During the 1988 opposition, this line was observed at 100 kHz resolution with the IRAM 30 m telescope. The 12″ FWHM beam of the facility allowed spatial resolution of the Martian disk (23″.8). The high S/N of the data allowed measurement of winds with a 1 σ absolute line-of-sight accuracy of 20 m s^{-1}. The measurements, performed during Southern summer solstice ($L_s = 279°$), stress the Southern hemisphere and clearly indicate a global easterlies flow. If modeled by a broad easterly jet with a maximum centered at 20 S, and extending 80° in latitude, the jet core velocity is found to have a χ^2 minimum at 160 m s^{-1} ($\pm$80 m s^{-1} at the 95% confidence level), generally consistent with predictions for broad summer easterly jets near 50 km as proposed by theoretical models. If the flow is modeled instead by a planet-wide solid rotator zonal flow which is restricted to the Southern hemisphere or equatorial regions, the velocity of the easterlies is nearly the same. These wind measurements, together with the temperature measurements of Deming et al., provide the first experimental rough picture of the middle atmosphere circulation of Mars, in general agreement with the Jaquin axisymmetric middle atmosphere model and the current Mars GCM model of Pollack et al.

Subject headings: planets: atmospheres — planets: Mars — radio sources: spectra

1. INTRODUCTION

While our knowledge of the dynamics of the lower atmosphere of Mars (0–50 km) has benefitted from extensive temperature measurements by the *Mariner 9* IRIS (Hanel et al. 1972) and *Viking* IRTM (Martin 1981), and from direct surface wind measurements by the *Viking* landers (Hess et al. 1977), an understanding of the circulation at higher altitudes (50–100 km) is presently limited by lack of observational constraints. The middle atmosphere circulation of Mars is believed to be quite similar to that of the Earth. On Earth, solstitial differential heating drives a mean meridional circulation with rising motion near the summer pole, a meridional drift at high levels into the winter hemisphere, and sinking motion near the winter polar mesopause. The Coriolis torques exerted on this meridional flow generate mean zonal eaterlies (retrograde) in the summer hemisphere, and westerlies (prograde) in the winter hemisphere (Leovy 1964; Holton 1975). A strong zonal friction force is additionally required to satisfy both the heat and momentum budgets of the terrestrial mesosphere (Lindzen 1981; Holton 1982, 1983; Holton & Zhu 1984). The mechanism producing such drag is believed to be the breaking, near the turbopause, of gravity waves generated in the Earth's troposphere by flow over topography, etc. This momentum stress (drag) due to breaking gravity waves appears to be primarily responsible for "closing off" the mesospheric jets at high altitude (both the westerly winter and the easterly summer), and for the reversal of the latitudinal temperature gradient in the upper mesosphere. Temperatures are thus lowest at the summer pole (due to adiabatic cooling from upwelling) and warmest at the winter pole (due to adiabatic heating from subsidence). In view of the large amplitude of Martian topography, gravity waves should play a role at least as important for the atmosphere of Mars as for that of the Earth.

Observational data related to the middle atmosphere dynamics of Mars are limited to temperature maps from heterodyne measurements of CO_2 10 μm lines performed during the 1984 opposition (Deming et al. 1986; Rothermel et al. 1988). The temperatures, averaged over the 50–85 km altitude range were found to vary greatly with latitude, with minimum temperatures (close to CO_2 radiative equilibrium) near the subsolar pooint, and strong warming (by 50–100 K over CO_2 radiative equilibrium temperatures) towards high latitudes in both the winter and summer hemispheres. As in the terrestrial case, the reversed winter hemisphere latitudinal temperature gradient is likely driven by dynamical heating in the winter polar region (Deming et al. 1986). The latitudinal symmetry of the observed temperatures is possibly due to increased radiative heating, especially at high summer latitudes, due to absorption by suspended dust (Haberle, Leovy & Pollack 1982). These measurements have been extremely useful to constrain dynamical models of the middle atmosphere of Mars (Jaquin 1989; Barnes 1990). However, they do not provide a straightforward picture of its wind system.

We report here the first absolute wind measurements in the middle atmosphere of Mars. They are based on inspection of Doppler shifts of the $J = 2$–1 ^{12}CO rotational line, mapped over the Martian disk during the 1988 opposition. A similar study has been successfully achieved for Venus by Pierce, Muhleman, & Berge (1991) (in $J = 1$–0 CO) and Buhl, Goldstein, & Chin (1991) (in $J = 2$–1 CO). The objective of our observations was in fact the spatial variability of Martian carbon monoxide abundance which was obtained from simul-

[1] Département de Recherches Spatiales, Observatoire de Paris–Meudon, 92195 Meudon, France.
[2] Laboratory for Astrophysics, National Air and Space Museum, Smithsonian Institution, Washington, DC 20560.
[3] Lunar and Planetary Laboratory, University of Arizona, Tucson, AZ 85721.
[4] Institut de Radio-Astronomie Millimétrique, Avda de la Divina Pastora, Granada, Spain.

taneous observations of the $J = 2–1$ ^{12}CO and ^{13}CO lines (Lellouch et al. 1991). However, the signal-to-noise ratio on the ^{12}CO 2–1 line appeared to be high enough to unambiguously detect Doppler shifts and to allow wind measurements with a typical 1 σ absolute accuracy of 20 m s^{-1}.

2. OBSERVATIONS

On 1988 September 23–25, we observed Mars in the $J = 2–1$ ^{12}CO and ^{13}CO rotational lines at 230 and 220 GHz, respectively, using the IRAM 30 m radiotelescope at Pico Veleta, Spain. The telescope was equipped with a SIS receiver characterized by a receiver noise temperature of about 250 K. Sky conditions were excellent (zenith opacity less than 0.1), allowing system temperatures of 500–600 K. Taking advantage of the narrow beam of the facility [about 12″ full width at half-maximum (FWHM) at 230 GHz], compared to the angular diameter of Mars (23.″8), we mapped the lines as a function of the position on the disk. Fourteen points were recorded, roughly corresponding to a sampling at half-beam. Since our observation was performed almost exactly at opposition, perihelion, and Southern summer solstice ($L_s = 279°$), the entire dayside of Mars was observed, spatial resolution was maximized and extensive coverage was achieved for the Southern hemisphere. The sampled latitudes extend from 60° N to 90° S, with five points recorded along the equator. The directions east and west mentioned throughout are planetary based. The ^{12}CO and ^{13}CO spectra were obtained by rapid position switching with the telescope secondary wobbling at 1 Hz. Observations were performed in double sideband, with the line located in the lower sideband. We used two filter banks, a 512 channel 1 MHz resolution bank and a 256 channel 100 kHz resolution bank. At 230 GHz, 100 kHz resolution corresponds to a line-of-sight (LOS) velocity resolution of 130 m s^{-1}. However, the signal-to-noise (S/N) allowed line centroiding to $\sim$15 kHz (1 σ) or 20 m s^{-1}.

The ^{12}CO $J = 2–1$ line at Mars is seen in absorption with a 25% depth and 20 MHz width, whereas the ^{13}CO line generally appears as a 3% absorption feature of 1 MHz width superposed on broader emission wings due to the lower atmosphere (nadir and limb) contribution. Because our first objective was to measure the CO abundance, for which the ^{13}CO line is the best tracer, most of the observing time was dedicated to achieve a satisfactory S/N on ^{13}CO. Our 100 kHz resolution observations of the ^{12}CO line, which contain the Martian winds information, are in fact limited to two 1 minute spectra for each of the 14 points. As detailed below, the probed altitudes extend from about 40 to 70 km. Although sufficient for an accurate retrieval of the CO abundance, the S/N on the ^{13}CO lines is not large enough to infer winds at lower altitudes.

To minimize pointing errors, which are critical in this kind of observation, the observations were generally performed as follows. The pointing was checked by azimuth and elevation continuum drifts across Mars. Then after a calibration procedure was performed, 1 minute integration scans were recorded successively at the 14 target points. Pointing and calibration were then rechecked, followed by a second set of scans at each point. The 100 kHz resolution observations of the ^{12}CO line were obtained when Mars elevation was between 51° and 42° (air mass 1.29 to 1.49). The estimated absolute pointing uncertainty, from residuals in continuum drifts, is 3″. Given the way the experiment was conducted, the pointing error is systematic i.e., the magnitude and direction of the offset are the same for all beam locations. The relative (offset) pointing and tracking uncertainty are estimated to be about 0.″5 each.

3. DATA REDUCTION AND MEASUREMENT OF BEAM-INTEGRATED WINDS

For each of the $^{12}CO(2–1)$ 100 kHz resolution spectra, a 1 MHz resolution spectrum was recorded simultaneously. This "low" resolution spectrum was used to define the continuum level. Baseline ripples, which are known to affect millimeter-wave spectra of planets, were eliminated by removing a first-degree baseline at low resolution, then applying the same baseline correction to the corresponding high resolution (100 kHz) spectrum. The baseline was always found flat over the 25.6 MHz bandwidth of the high-resolution spectrum.

In the Lellouch Paubert, & Encrenaz (1991) analysis, the individual ^{12}CO and ^{13}CO spectra were rescaled to their continuum levels, and then averaged by position offsets without any further treatment. This allowed us to infer, for each beam position, the local CO mixing ratio and vertical thermal structure, In particular the uncertainty on the retrieved thermal structure was about 20 K, primarily due to the uncertainty on the local surface temperature.

Accurate wind measurements from Doppler shifts in the $^{12}CO(2–1)$ line center requires fine frequency corrections to the data and improved modeling. The real-time software at IRAM, before each scan, computes the total velocity of the source with respect to the telescope (Earth-Mars translation plus Earth's rotation), and adjusts the local oscillator (LO) frequency accordingly. While the LO, in principle, refers the spectra to the barycentric frame of Mars, its step size is exactly 24.48 kHz, which means that the sky frequency cannot be synthesized with an absolute accuracy better than $\pm$12.24 kHz. This limitation was overcome by recomputing Mars-IRAM relative velocity at the time of each scan, comparing the required LO frequency with its true value, and shifting the frequency scale of the scan by the appropriate fractional number of channels. Each pair of 100 kHz spectra for each beam position were then averaged.

The Doppler shifts were obtained by cross-correlating the observed averaged spectra within $\pm$1 MHz of line core (over 20 high-resolution channels) with synthetic profiles generated by a radiative transfer model, using the local CO and thermal structure measurements of Lellouch et al. (1991). Absolute wind velocity determination is limited by both the accuracy of the rest frequency for the 2–1 transition and the value of the pressure shift in CO by CO_2. We adopted the recently measured values of 230538.000$\pm$0.001 MHz ($\pm$1.3 m s^{-1}) and +18 kHz/torr (at 180 K), respectively (S. P. Belov et al. 1991 private communication). Both were incorporated into the radiative model which was otherwise identical to that of Lellouch et al. (1991). The pressure shift at the level where the line core is formed [about 3 μbar (70 km)] is negligible. Superposition of the core onto pressure-shifted wings was found to induce a minor core shift of 1 kHz (1.3 m s^{-1}). Retrieved lineshifts are relatively insensitive to the exact shape of the reference profile (e.g., Pierce et al. 1991), therefore are very little affected by the radiative transfer model uncertainties. By successively measuring the shift at a given point of the map using synthetic profiles corresponding to various other points, we estimated this effect to be at the 1–2 m s^{-1} level.

In addition, fitting was also independently performed to the data (1) within $\pm$0.35 MHz of line core, and (2) in the $\pm$(0.35–1

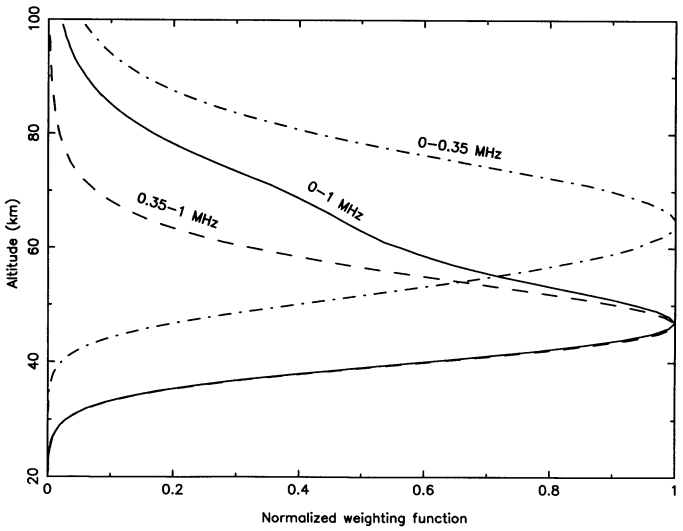

FIG. 1.—Average weighting functions in the ^{12}CO $J = 2$–1 line at 230.538 GHz, computed for a CO mixing ratio of 8×10^{-4} and the observing geometry of the subearth point.

MHz) spectral region, in an attempt to derive vertical wind velocity information. In each of the three cases, the best model fit was obtained by shifting the synthetic spectrum along the observed by steps of 1 kHz, and the standard deviation, σ, of the data from this best model was computed. Random noise at the obtained σ level was then generated, superposed on the best model and the resulting distribution was refit. After 20 repetitions, the standard deviation in the offset from line rest frequency was computed. In addition to the spectroscopic uncertainties mentioned earlier, systematic errors due to the accuracy of the ephemeris (≤ 1 m s^{-1}) and to a gravitational blueshift (1 m s^{-1}) are negligible.

In order to assign altitude levels for the wind measurements, the temperature weighting functions were computed for an average mixing ratio of 8×10^{-4} and the observing geometry at the subearth point. The weighting functions at 0, 0.35 and 1 MHz from line center peak at 71, 55, and 42 km, respectively, with half-power widths of 21, 18, and 13 km, respectively. Averaging the weighting functions between 0 and 1 MHz from line center shows that the 0–1 MHz interval provides information on levels between 39 and 63 km altitude (the half-power altitudes for the averaged weighting functions). Similarly, the 0–0.35 and 0.35–1 MHz intervals probe the 52–78 km and 39–56 km ranges, respectively (Fig. 1). Although it would be of obvious interest to extend measurements further into the line wings, the flatness of the line shape beyond 1 MHz from line center prevents retrieval of meaningful shifts at lower altitudes. For example, the 1 σ uncertainty on winds measured between 1 and 4 MHz from line center (probing the 25–42 km altitude range) would be typically 60 m s^{-1}.

4. RESULTS

4.1. *Qualitative Analysis*

Table 1 gives the *beam–integrated* Doppler shifts (expressed in m s^{-1}, positive for recession) measured over the three intervals: 0–1, 0–0.35, and 0.35–1 MHz from line center. The corresponding 1 σ wind uncertainties are 21, 25, and 30 m s^{-1} on average. As examples, spectra recorded along the Martian equator are shown in Figure 2, along with their best model fits.

Figure 3 shows the LOS projected winds measured in the 0–1 MHz range, after correction for beam–integrated Mars solid planet rotational components, as detailed below. Immediately evident, particularly in the Southern hemisphere, is a general zonal easterlies flow characterized by approach in the east, near zero LOS velocities across the subearth meridian and recession in the west. Beam position 4 near the South pole, with a strong blueshift cannot be interpreted in terms of a purely zonal field and was therefore omitted from the modelling. Although in principle, comparison of points off the central meridian can reveal information about latitudinal variations, the large beam was found to preclude such studies here. Finally, inspection of Table 1 does not reveal any obvious variation of the circulation with altitude at the vertical resolution considered.

4.2. *Dynamical Modeling*

A retrieved wind velocity reflects dynamical contributions from all regions intercepted by the beam. Modeling of these *beam-integrated* wind velocities is therefore required for a quantitative detrmination of the global wind field responsible.

TABLE 1

OFFSET MEASUREMENTS[a]

Point	Latitude	Longitude[b]	0–1 MHz	0–0.35 MHz	0.35–1 MHz
1.....	−21	0	−1(12)	16(13)	−18(13)
2.....	0	90	−60(26)	−20(17)	−97(59)
3.....	0	−90	87(27)	96(39)	81(31)
4.....	−90	0	−120(27)	−210(44)	−98(29)
5.....	60	0	−9(20)	−18(23)	−5(29)
6.....	0	0	−13(16)	−6(19)	−25(17)
7.....	0	35	−57(19)	−73(32)	−38(21)
8.....	0	−35	60(18)	61(25)	38(23)
9.....	−35	0	12(14)	35(21)	−13(25)
10.....	25	0	7(12)	16(13)	−25(19)
11.....	−35	45	−45(32)	−57(31)	−53(41)
12.....	−35	−45	5(27)	20(28)	−13(40)
13.....	25	60	−116(23)	−114(43)	−118(38)
14.....	25	−60	44(21)	73(20)	−21(28)

[a] In m s^{-1}; positive offsets indicate recession; brackets: 1 σ uncertainty.
[b] Positive planet westward from the central meridian.

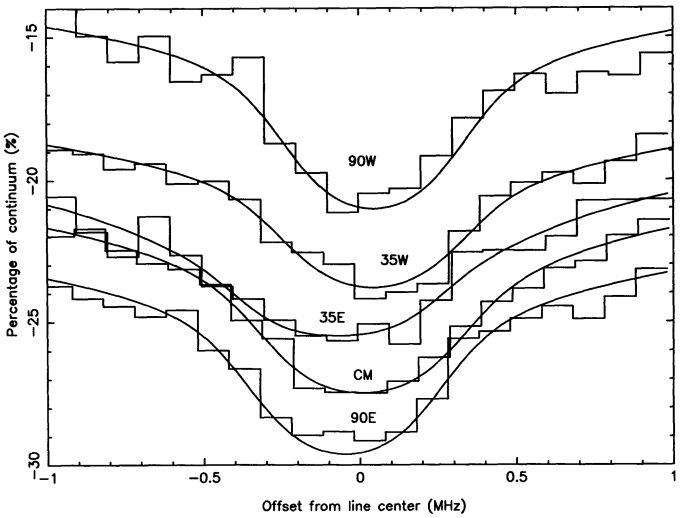

FIG. 2.—Line cores observed along the Martian equator (*histograms*) compared to best-fit models (*solid lines*). The line center is assumed to be at 230.538000 GHz. The line absorption is expressed in continuum units. "CM" indicates central meridian. Longitudes are measured from the CM..

Modeling of the retrieved winds was accomplished (as per Goldstein et al. 1991; Goldstein 1990) by assuming a global, zonal wind field superposed on the solid planet rotation of Mars (242 m s^{-1} at the equator) and convolving the Doppler shifted line contributions over the entire beam. The zonal field was initially assumed to be a solid body rotator (horizontal velocity is proportional to the cosine of the latitude). Vertical velocities were assumed everywhere zero. A model space was generated by modeling the beam-integrated winds for different zonal wind strengths. Goodness-of-fit between the *ensemble* of modeled and observed velocities allows model wind field discrimination.

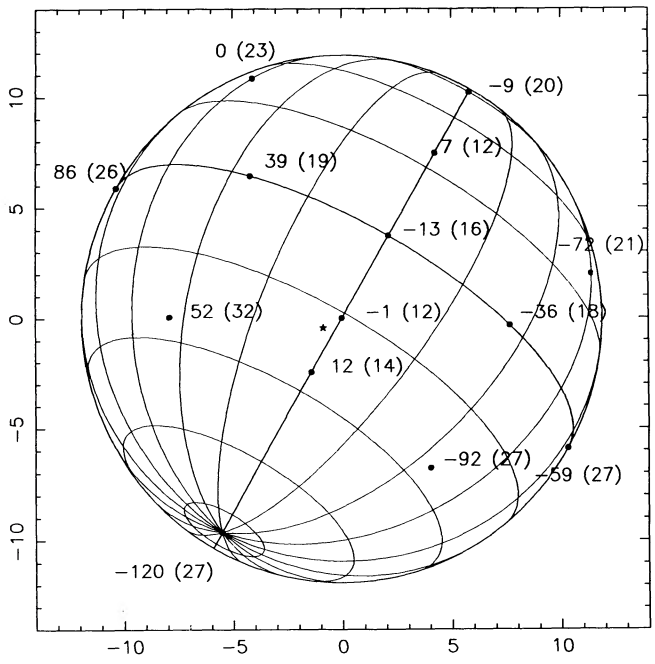

FIG. 3.—Line-of-sight beam-averaged winds (m s^{-1}) at 39–63 km (measured between 0 and 1 MHz from line center). The Doppler shifts have been corrected for the solid rotation of Mars. Positive winds indicate recession. The number in brackets indicates the 1 σ uncertainty. The star locates the subsolar point.

The beam was partitioned into a 100 × 100 element grid, with a beam diameter twice the diffraction-limited FWHM (12″). Within each beam element, horizontal wind velocity, LOS projection geometry, and beam spatial roll-off were taken as constant and evaluated at the element centroid. Each element produces a line contribution, frequency translated by the appropriate LOS velocity, as dictated by the model wind field. The contribution's relative weight is determined from the beam roll-off and element area. The element contributions were spectrally summed, and the frequency (velocity) centroid of the convolution was defined as the LOS beam-integrated velocity. Martian solid rotation components used to generate Figure 3 were obtained through beam modeling with the wind field removed.

Model goodness-of-fit was determined from the (error bar weighted) dispersion S between the N observed and modeled wind velocities, in units of the mean error bar (Goldstein 1990). A minimum S near unity indicates a good model fit with a dispersion attributable to the rms noise in the data. However, for small N, a model space about the minimum exists within which models are statistically indistinguishable. Quantitative description of this "best-fit model space" was obtained using the χ^2 test. A 95% confidence level best-fit model space was adopted, outside which the χ^2 probability of obtaining the observed S through statistical fluctuations is $\leq 5\%$. This required, for $N = 13$ retrieved wind velocities, that S be less than 1.3.

Regarding the ± 1 MHz data, a number of model spaces were generated with zonal wind fields of varying latitudinal (β) extent and parameterized by equatorial velocity V_{eq}. As detailed in Table 2, the observed data could only be adequately fit by a definitive easterly flow that must at least exist in tropical to mid Southern latitudes. For the planet-wide case ($-90° \leq \beta \leq 90°$), $V_{eq} = 110 \pm 55$ m s^{-1}. The error reflects the extent of the 95% confidence level model space. Restricting the wind field to Southern latitudes or the tropics boosts the strength of V_{eq} by 50–75 m s^{-1} (on average). Restricting the wind field to Northern latitudes yields a minimum $S = 1.4$, precluding a fit to the data.

Another characterization of the zonal wind field was attempted, more in line with current simulations of easterlies near 50 km from the Mars general circulation model (GCM) (Pollack et al. 1990) and a Mars climate model under development (J. R. Barnes 1991, private communication). See discussion below for details. A broad summer easterly jet with a sinusoidal rolloff was assumed, characterized by a maximum centered at 20S and zeros at 20N and 60S. Only the jet's core velocity was allowed to vary to obtain a best-fit model. The model space minimum occurs for a jet core velocity at 20S of 160 ± 80 m/s, much the same as the restricted Southern latitude (case 2) and tropical (case 4) zonal flow models above (see Table 2).

The nominal beam positions were then offset by the 3″ worst case pointing uncertainty East, West, North, and South on the planet, to determine the effects on the best-fit model spaces. East and West offsets produced model spaces unable to fit the data: beam-integrated velocities of 20–30 m s^{-1} were obtained at positions along the subearth meridian, inconsistent with the observed (Fig. 3). Pointing uncertainty if indeed present at the 3″ level, must therefore have been predominantly North–

TABLE 2

EQUATORIAL VELOCITIES FOR THE ZONAL FLOW MODELS

Case Number	Fitting Interval (MHz)	Latitude Range of Zonal Flow	Best-Fit Model Space V_{eq}(m s^{-1})[a]	Minimum χ^2 Model V_{eq}(m s^{-1})
1.....	0–1	$-90° \leq \beta \leq 90°$	55 to 165	110
2.....	0–1	$-50 \leq \beta \leq 0$	85 to 290	185
3.....	0–1	$0 \leq \beta \leq 50$	...[b]	...[b]
4.....	0–1	$-20 \leq \beta \leq 20$	100 to 230	160
5[c].....	0–1	$-60 \leq \beta \leq 20$	80 to 240	160
6.....	0–0.35	$-90 \leq \beta \leq 90$	115 to 170	145
7.....	0.35–1	$-90 \leq \beta \leq 90$	105 to 195	150

[a] Positive velocities indicate easterlies.
[b] No acceptable model space.
[c] Sinusoidal rolloff centered at 20 South and zeros at 20 North and 60 South (consistent with Pollack et al. 1990).

South. However, North and South offsets were found to have no effect on the model spaces of Table 2.

Finally, model spaces were generated independently for the 0–0.35 MHz and 0.35–1 MHz data. The acceptable ranges in V_{eq} (Table 2) overlapped the 0–1 MHz data, indicating that the easterly flow exists in both the 39–56 km and 52–78 km altitude ranges, though wind strength variation with altitude could not be discerned.

Regarding the Table 2 cases, while the magnitude of the χ^2 uncertainty is high, the signature of a strong easterly flow is clearly evident, and allows coarse comparison to dynamical models.

5. DISCUSSION

Theoretical models of the Mars middle atmosphere are at a very early stage of development, owing to limited atmospheric data sufficient to provide usable constraints. However, the detection of polar warming at 50–85 km altitude (Deming et al. 1986; Rothermel et al. 1988) prompted the development of simple dynamical models to estimate the likely role of gravity wave drag on the circulation of the Mars middle atmosphere (Jaquin 1989; Barnes 1990). Also, Mars GCM model fields are now being calculated up to nearly 50 km, thereby providing a crude estimate of middle atmosphere zonal winds (Pollack et al. 1990).

The thesis work of Jaquin (1989) adapted a two-dimensional, linearized, axisymmetric formulation of the equations of motion (Leovy 1964) to Mars. His code made use of calculated radiative equilibrium temperatures, Rayleigh friction and Newtonian cooling time scales (as a function of log pressure) to drive the Mars model circulation. From simulation of the growth and breakdown of gravity waves over realistic Martian terrains, the wave breaking level, on a global average basis, was set at 50 km, and the derived Rayleigh friction time constant above 50 km was 1 day, much less than the Newtonian cooling time constant. The velocity fields obtained indicate that the Mars middle atmosphere is characterized by a pole-to-pole circulation at the solstices, and an equator-to-pole circulation at the equinoxes. As in the terrestrial mesosphere, the Coriolis torques exerted on this meridional flow generate mean zonal easterlies (retrograde) in the summer hemisphere, and westerlies (prograde) in the winter hemisphere. Zonal wind speeds in the core of the winter zonal jet, being nearly 10 times faster than the meridional winds, are on the order of 80 m s^{-1}, with the jet centered near 60° latitude and about 45 km. The summer easterly zonal jet is weaker, broader in latitudinal extent, and its core is closer to the equator.

The Barnes (1990) model formulation is somewhat more realistic in that the wave breaking level (where wave drag effects maximize) is allowed to vary with season. His results indicate that the Deming et al. (1986) picture of the Mars thermal structure in the 50–85 km region, with both poles warm and the tropics cold, corresponds to a relatively low-level (50 km) winter westerly jet and a relatively high (85 km) summer easterly jet. In the winter hemisphere, plausible mesoscale gravity waves, generated by flow over topography, seem able to force the closure of the westerly jet in the 40–80 km region. The corresponding meridional circulation acts to produce very warm winter polar temperatures at these altitudes with values 50 K above radiative equilibrium, comparable to those seen by Deming et al. (1986). The core of the winter westerly jet (channel center at 60° latitude) is obtained at 50 km, with a wind speed of about 150 m s^{-1}. The zonal wind decreases very sharply above this level to values of about 25 m s^{-1} at 80–90 km, where meridional winds become appreciable.

In the summer hemisphere, "filtering" by low atmosphere (below $\sim$15 km) westerlies is especially effective in keeping stationary waves (forced by flow over topography) from propagating into the middle atmosphere. Results indicate that gravity waves might force the closure of the summer (easterly) jet at higher levels than in the winter hemisphere. In the 50–80 km region, summer high latitudes might be warm, as indicated by Deming et al. (1986). The summer pole would be cold only at still higher altitudes due to adiabatic cooling. Nominal summer zonal winds peak at 85 km, with easterly wind speeds of 130 m s^{-1}; winds at 50 km are on the order of 100 m s^{-1}, somewhat weaker than the corresponding winter hemisphere westerlies.

Both of these models specifically address the Mars middle atmosphere dynamics. However, they are based upon the simplified equations describing the winds. Lower atmosphere circulation models are available that are based upon the full-blown primitive equations and Mars radiative, chemical, and dust formulations. These models include a general circulation model—GCM (Pollack et al. 1990) that calculates three-dimensional fields over the globe on a rather coarse grid from the ground up to 47 km. A higher resolution Mars climate model is under development, using somewhat elementary infrared physics, simulating winds up to 55 km (Barnes 1991, private communication). Both of these models predict relatively weak summer zonal easterlies (compared to the

westerlies), with ~ 120 m s^{-1} maximum velocities near 50 km. These jets do not appear to be "closing off" at the model upper boundaries where a "sponge layer" is assumed for numerical stability. However, the basic structure of the easterly flow pattern is a summer jet with a core near 20–25 South latitude and easterlies extending over a broad latitude range from 60 South to 20 North latitude. The winds measured here at 40–70 km, when characterized by a sinusoidal latitudinal distribution centered at 20 South (60 South to 20 North), yield a core speed of 160 ± 80 m/s, generally consistent with the Pollack et al. (1990) GCM simulations.

Due to the poor coverage of the Northern hemisphere, our observations cannot firmly establish the direction nor the strength of the wind there. Specifically, models with and without winds in the Northern hemisphere fit the data equally well. Therefore theoretical models, predicting the intrusion of summer easterlies into the winter hemisphere (as is common in the terrestrial middle atmosphere; Holton 1975) and the closure of the winter westerly jet remain to be observationally tested.

On the whole, these wind measurements combined with the temperature measurements of Deming et al. (1986) appear consistent with current theoretical models. The CO millimeter-wave measurements also provide the mapping of the atmospheric temperature. For a coherent picture of the middle atmosphere dynamics, the winds inferred here at 40–70 km should be viewed in the context of derived latitudinal temperature variations. This unfortunately does not give convincing results because (1) in the absence of absolute calibration the retrieved temperatures are uncertain by ± 20 K (Lellouch et al. 1991) and (2) the large size of the beam considerably smears out any temperature latitudinal contrast, especially in the Northern hemisphere.

Finally, the beam–integrated wind velocity at point 4, inconsistent with a zonal flow, can be interpreted as a high-velocity meridional component restricted to the South polar region. The beam–integrated blueshift is consistent with equatorialward transport. Meridional velocities of this magnitude (≥ 100 m s^{-1}) seem high, yet need to be validated using theoretical models for Mars conditions of this particular time period.

Future observational progress on the middle atmosphere of Mars dynamics requires simultaneous measurement of the temperature and wind velocities. Infrared heterodyne measurements at 10 μm obtained during the 1988, 1990 oppositions, admitting tenfold better spatial resolution than the microwave, are ideally suited for this study (Goldstein et al. 1991, in preparation). Additionally, existing GCMs will have to be extended to significantly higher altitudes.

We are indebted to Fred Espenak for kindly computing the Martian ephemeris. We also thank Jeff Barnes and Jim Pollack for illuminating discussions. J. J. G. was supported by a grant from the Smithsonian Institution Scholarly Studies Program.

REFERENCES

Barnes, J. R. 1990, J. Geophys. Res., 95, 1401
Buhl, D., Goldstein, J. J., & Chin, G. 1991, ApJ, submitted
Deming, D., et al. 1986, Icarus, 66, 366
Goldstein, J. J. 1990, NASA CR 4290, Absolute Wind Measurements in the Lower Thermosphere of Venus using Infrared Heterodyne Spectroscopy, (Washington, DC: GPO)
Goldstein, J. J., et al. 1991, Icarus, submitted
Haberle, R. M., Leovy, C. B., & Pollack, J. B., 1982, Icarus, 50, 322
Hanel, R., et al. 1972, Icarus, 17, 423
Hess, S. L., et al. 1977, J. Geophys. Res., 82, 4559
Holton, J. R. 1975, Meteorological Monographs, Vol. 15, No. 37, The Dynamic Meteorology of the Stratosphere and Mesosphere (Boston: Amer. Meteorological Society)
Holton, J. R. 1982, J. Atmos. Sci., 39, 791
———. 1983, J. Atmos. Sci., 40, 2497
Holton, J. R., & Zhu, X. 1984, J. Atmos. Sci., 41, 2653
Jaquin, R. F. 1989, Ph.D. thesis, Cornell University
Lellouch, E., Paubert, G., & Encrenaz, T. 1991, Planet Space Sci., 39, 219
Leovy, C. B., 1964, J. Atmos. Sci., 21, 327
Lindzen, R. S. 1981, J. Geophys. Res., 86, 9707
Martin, T. Z. 1981, Icarus, 45, 427
Pierce, K., Muhleman, D. O., & Berge, G. L. 1991, Icarus, in press
Pollack, J. B., Haberle, R. M., Schaeffer, J., & Lee, H. 1990, J. Geophys. Res., 95, 1447
Rothermel, H., Kaufl, H. U., Schrey, U., & Drapatz, S. 1988, Astron. Astrophys., 196, 296